Preliminary Tests of HIKHET Laboratory Model at IFPiLM

IEPC-2019-591

Presented at the 36th International Electric Propulsion Conference
University of Vienna • Vienna, Austria
September 15-20, 2019

Jacek Kurzyna[1], Maciej Jakubczak[2], Agnieszka Szelecka[3] and Arsenii Riazantsev[4]
Instytut Fizyki Plazmy i Laserowej Mikrosyntezy (IFPiLM), Hery 23, Warsaw, 01-497, Poland

Abstract: This paper presents the major results from the measurement campaign of a krypton Hall Thruster first prototype developed under project HIKHET at IFPiLM. This 500 W-class Hall Thruster was operated in a wide range of krypton mass flow rates (0.6 to 1.0 mg/s), discharge voltages (240 to 800 V), and magnetic field settings to identify conditions in which high specific impulse (over 2000 s) can be achieved. Thruster performance (discharge current, thrust production, anode efficiency) as well as some ion characteristics (ion current density angular distribution, mean ion velocity) are shown, and possible sources of performance reduction are discussed.

Nomenclature

b	=	channel width
g_0	=	standard gravity
I_d	=	discharge current
I_e	=	electron current
I_i	=	ion current
I_m	=	maximum current of singly-charged ions for the given mass flow rate
I_{sp}	=	specific impulse
l_s	=	sheath length
$\dot{m}_a$	=	anode mass flow rate
P_d	=	discharge power
T	=	thrust
U_d	=	discharge voltage
η_a	=	anode efficiency

I. Introduction

HALL Thruster, with more than half century of development, is currently one of the most matured Electric Propulsion (EP) technologies available for spacecraft. Nevertheless, despite many years of research and the already huge progress made in this field, nowadays there are still tens of public and private-funded laboratories all over the world that focus their effort on further understanding and advancement of this technology.

The reason is obvious – from the perspective of a spacecraft two most important aspects of a propulsion system i.e. high effective exhaust velocity of the propellant and small mass of the system (that includes thruster itself, power supplies and gas management system) are offered by HT. Both govern the overall mass budget of a space mission. Moreover, HT is relatively simple device which could be manufactured in a better equipped workshop. It achieves

[1] Research Fellow, Department of Plasma Diagnostics and Technology, jacek.kurzyna@ifpilm.pl.
[2] Research Assistant, Department of Plasma Diagnostics and Technology, maciej.jakubczak@ifpilm.pl.
[3] Research Assistant, Department of Plasma Diagnostics and Technology, agnieszka.szelecka@ifpilm.pl.
[4] Research Assistant, Department of Plasma Diagnostics and Technology, arsenii.riazantsev@ifpilm.pl.

high anode efficiency η_a which in case of powerful thrusters operating with xenon (like SPT-290, NASA-300M, NASA-457M and others) gains ~70 %, produces thrust-to-power (T-to-P) ratio of the order of 50 mN/kW and specific impulse I_{sp} which varies from 1500 up to 3200 s or more[1]. While those HTs of the highest power are targeted towards orbit transfer maneuvers, driving open space probes or even interplanetary missions also small satellites request for effective electric propulsion, e.g. for attitude control and station keeping – especially when operating at LEO or within satellites formation. The scaling down of HTs to electric power attainable on board of the smallest spacecraft[2], results in engines of 0.1-0.5 kW class or even lower[3]. Unfortunately, continuously refined scaling-down relations (compare e.g. Refs. 4 and 2) show that size and power reduction leads unavoidably to performance degradation – mostly in terms of efficiency as well as I_{sp} production. This effect, among others, is an outcome of the increased surface to plasma volume ratio causing relative growth of thermal loss at the channel walls, higher electron current I_e share in the total discharge current I_d, increased ratio of the sheath thickness l_s to channel width b, increased channel wall erosion etc. Consequently, to "wring" the highest efficiency from HT technology more insight into its physics must be provided, just to mention a still open problem of anomalous electron transport coupling with microinstabilities growth, for which understanding, in addition to theoretical studies, an extensive experimental examination as well as modeling are steadily required.

In terms of mass budget I_{sp} increase is a crucial task to be worked out bearing in mind any propulsion technology. For HT a natural path for completing this goal is rise of discharge voltage as well as reduction of molecular mass of the expelled particles. The latter objective is a part of long-lasting effort to find an alternative to xenon propellant[5,6], according to which krypton, with its atomic mass M_{Kr}=83.8 u (while M_{Xe}=131.3 u) could be an interesting candidate. Nevertheless, due to smaller ionization cross section and higher ionization energy of krypton HT supplied with this propellant has to be less efficient than the same thruster fueled with xenon, what was already extensively discussed and experimentally verified[7-9]. On the other hand, there were only few papers reported in which small HTs were supplied with krypton propellant and operated at high voltage[10,11].

Several years ago in IFPiLM a laboratory model of 500 W-class Hall thruster was designed with aim at optimization for krypton propellant. The geometry of this thruster with respect to the well-known SPT-100 model was chosen relying on the "radial scaling" rule[4]. Within the ESA HIKHET (High Impulse Krypton Hall Effect Thruster) project that is currently under implementation in IFPiLM this thruster shall be adapted for operation with increased discharge voltage for high I_{sp} production. In this paper the results of a vast measurement campaign for the first HIKHET prototype performance assessment are presented.

II. Experiment set-up

All the tests have been performed in the IFPiLM's electric propulsion laboratory – PlaNS. Within the current section thruster itself, vacuum facility and diagnostics used will be briefly presented.

A. Thruster

The 500 W-class Hall thruster used in this study is a laboratory version which builds on KLIMT that was designed from scratch in IFPiLM and targeted for operation with krypton. KLIMT was already presented in details in our previous papers[12,13] and cited there literature to which the reader is kindly referred, and here only its most important features will be highlighted. The thruster geometry relies on the classic magnetic layer HT configuration[14] in which inner coil, annular discharge channel (made of boron nitride ceramics graded M26) and external coil make a concentric system. Perfect cylindrical symmetry is distorted only by a hollow cathode (HWPES-250 HeatWave Labs Inc. model[*]) that is fixed to the radiator externally with respect to the outer part of the magnetic circuit, see Fig. 1.

The length of the channel can be adjusted by shifting stainless steel anode that is simultaneously gas distributor in which two sets of circumferentially positioned orifices with diameter of 0.1 mm are covered with gas scattering baffles. The basic thruster parameters are shown in Table 1.

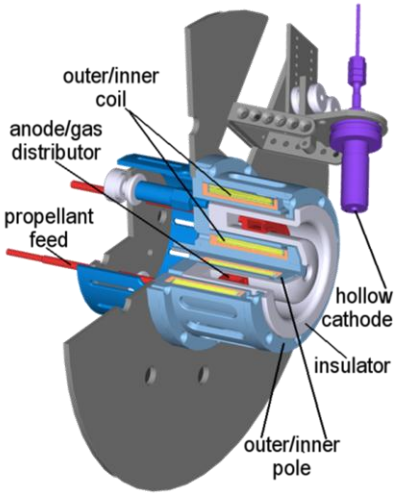

Figure 1. KLIMT cross section relevant to basic configuration: cap&collar BN insulator.

[*] HeatWave Labs, Inc., www.cathode.com

Table 1. KLIMT's basic parameters.

D_{inn} = 34 mm	D_{out} = 50 mm	b = 8 mm	L_{ch} = 12-25 mm	B_r^{max} = 150-250 Gs

Table 2. Thruster configuration for HV tests.

Basic configuration	Inner pole: 4 mm thick	Outer pole: 4 mm thick	Cap&colar insulator
Final configuration	Inner pole: 2 mm thick	Outer pole: 2 mm thick	plain insulator

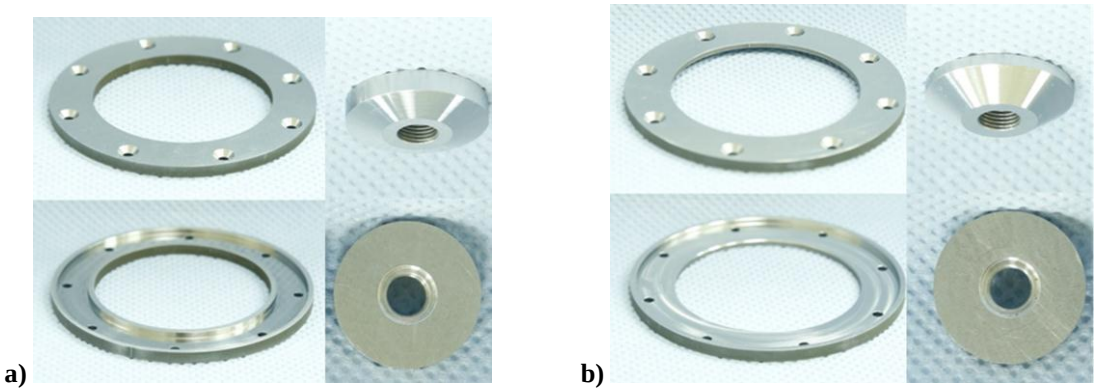

a) **b)**

Figure 2. a) Thick and thin b) convertible magnetic poles.

Design of the thruster magnetic circuit allowed for use of convertible poles as well as replacement of the main insulators. Consequently such hardware parameters as magnetic circuit, channel shape and length as well as the cathode position with respect to the channel exit plane and thruster axis were varied during the tests. Two sets of magnetic poles applied are depicted in Fig. 2 while two types of the main BN insulators used in the course of the measurement campaign are shown in Fig. 3.

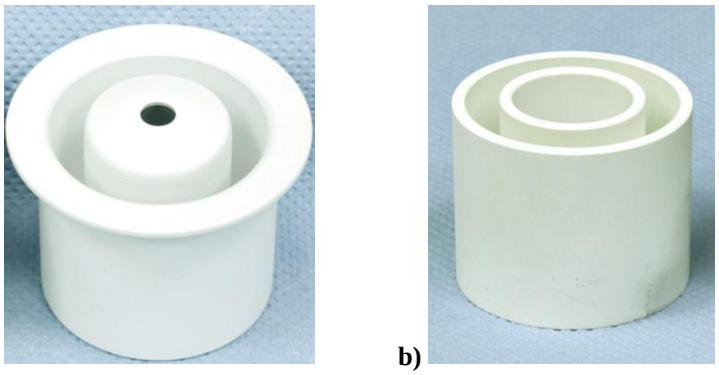

a) **b)**

Figure 3. BN insulators: a) cap&colar type and b) plain type.

The initial hardware configuration that corresponds to the KLIMT's genuine design will be further refereed as *basic* one, while the optimized configuration that was elaborated due to series of experiments as the *final* one. The key parameters of both configurations are summarized in Table 2.

For operation at increased discharge voltage an insulation of Kulgrid 28 wire[*] (that was used for KLIMT coils) appeared to be too fragile. That is why it was replaced with pure copper wire in fiberglass sleeve what reduced the highest allowable temperature of the coils down to 450°C for operation in long term scale and to ~500°C for short time scale operation. This solution, due to decreased packing factor of the coil windings, requires increased coil currents for generation the same magnitude of B-field as it was for KLIMT. As it was said in our previous papers[12,13] the basic magnetic field topography corresponds to photographic scaling down of the typical SPT-100 B-field distribution. A comparison of magnetic field topography as measured with RX-25 Hall effect 3D teslameter[†] and resulting due to finite element modeling with ANSYS Maxwell is shown in Fig. 4, while calculated evolution of magnetic field topography with variation of coil current ratios in Fig. 5.

[*] Ceramawire High Temperature Magnet Wire, http://www.ceramawire.com/technical-information.shtml#2

[†] Resonance Technology, http://www.resonance-technology.com/en/node/21

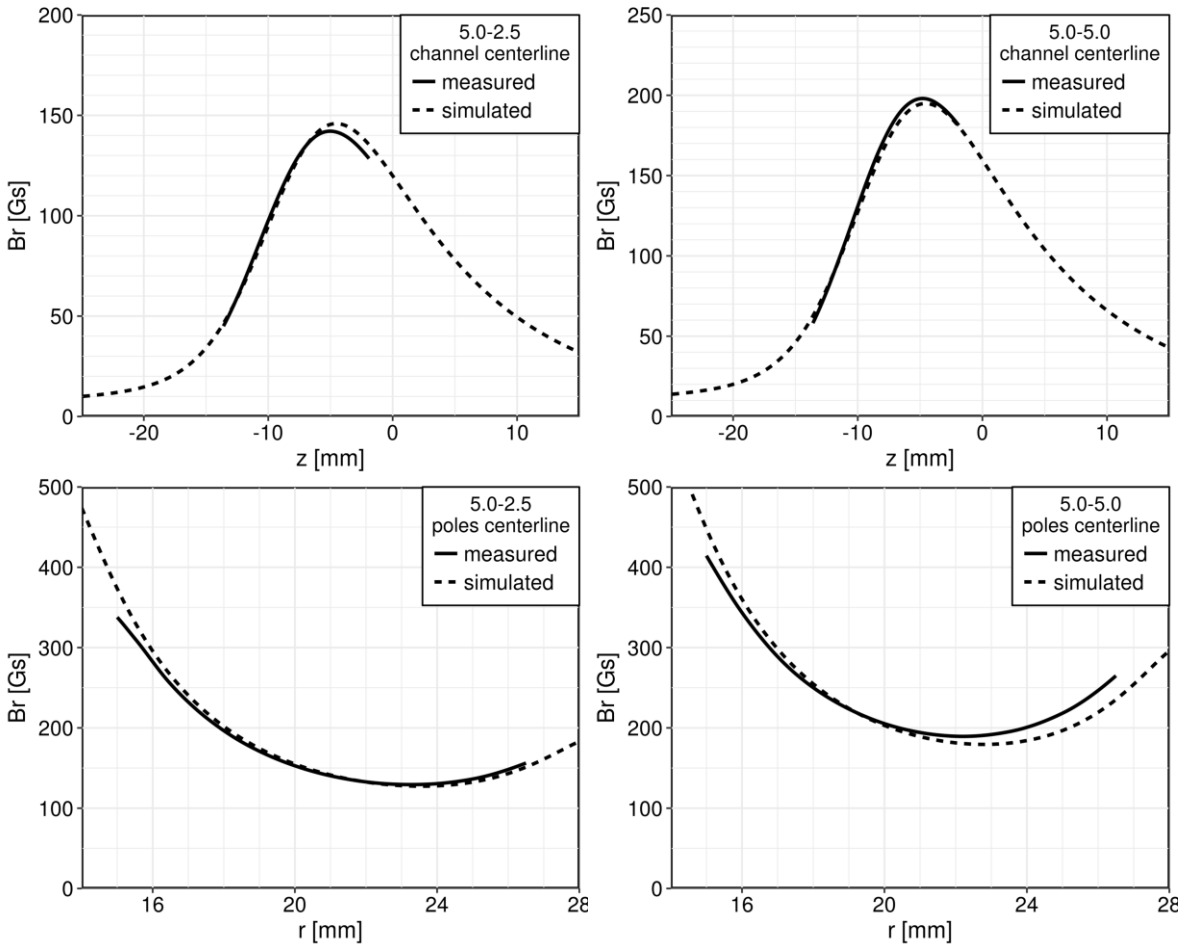

Figure 4. Magnetic field radial component profiles along the channel centreline (top) and poles centreline (bottom) for coil-current ratios 5.0-2.5 (left) and 5.0-5.0 (right). Dashed lines simulated with ANSYS Maxwell and solid lines measured with 3D teslameter.

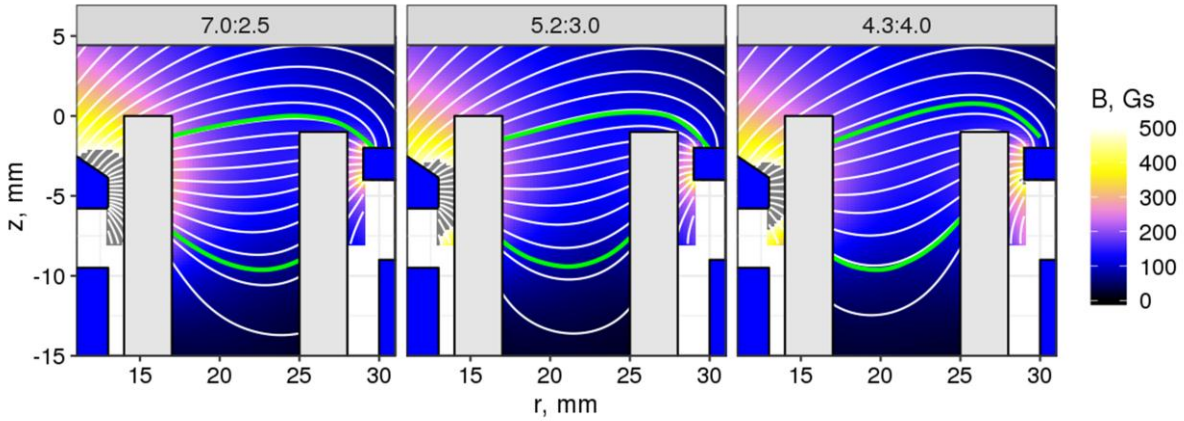

Figure 5. Topography of magnetic field inside the channel for different inner to outer coil current ratios (indicated at the top of each panel). Green profiles indicate predicted limits of the ionization-acceleration zone according to Ref. 15 and 16.

B. Vacuum chamber and power units

The thruster was installed in a cylindrical vacuum chamber at the thrust stand that was designed by Swiss MECARTEX company. The thrust balance will be described in some details in the next subsection. The vacuum chamber parameters and pumping system efficiency are collected in Table 3 – please note that overall pumping speed as measured for the whole facility equals ~14 m^3/s for xenon and ~18 m^3/s for krypton in the whole range of examined mass flow rates. During experiments with the thruster operating at different working conditions the pressure inside the chamber varied between 1 to 3×10^{-5} mbars (the figures are Xe or Kr corrected values as measured with Ionivac Oerlikon-Leybold ITR 90 vacuum gauge).

Table 3. Vacuum facility parameters.

Chamber and pumps		***Rate***	***Gas***
Length	~2.3 m		
Diameter	~1.2 m		
Volume	~2.5 m^3		
Backing pump	Adixen ACG 600 Multistage Roots	450 m^3/h	Air
TM pump	Pfeiffer HiPace 3400 MC	2.8 m^3/s	Air
Cryogenic pump	HSR Velco 900Xe	36 m^3/s	Air (N_2)
		34 m^3/s	Xe
		43 m^3/s	Kr

The thruster discharge voltage as well as the cathode keeper current was controlled with stabilized Sorensen SGI-1000/5 and SGI-800/6 power units. For cathode keeper and both magnetic coils current stabilized units Sorensen XG40-21 and 2×XG20-40 were used.

For mass flow rate stabilization in the anode and cathode lines the Sierra Instruments controller SmartTrak C100L and MicroTrack C101 calibrated for xenon and krypton were applied, both with declared 1% full scale accuracy. The pressure in the gas supply lines was measured with two membrane Oerlikon Ceravac CTR-91 gauges.

C. Thrust stand

For measurement of the impulse bits generated by a pulsed plasma thruster (PPT) supplied with liquid propellant a new type of thrust balance (TB) had been designed and manufactured[*] during implementation of EC FP7 project No. 283279[†]. The sensitivity of this TB allows to measure impulse bit value at the level of even single micro newton seconds. The concept[17] relies on the damped oscillator notion in which horizontal displacement of a pendulum (that consists of the thruster itself and its support) is measured to determine the force. The pendulum is suspended at a set of flexures with very high stiffness in the direction of gravity vector and very small one that is perpendicular to it. For better adjustment of the TB sensitivity to magnitude of the measured impulse bit one is able to vary horizontal stiffness of the flexures. According to the initial concept each impulse bit generated by a pulsed plasma thruster had to be followed by a calibrating pulse. In case of HT, which in contrary to PPT operates continuously, impulse bit generation was mimicked by switching-off the thruster. The thruster as installed at the thrust balance inside the IFPiLM's vacuum chamber is shown in Fig. 6.

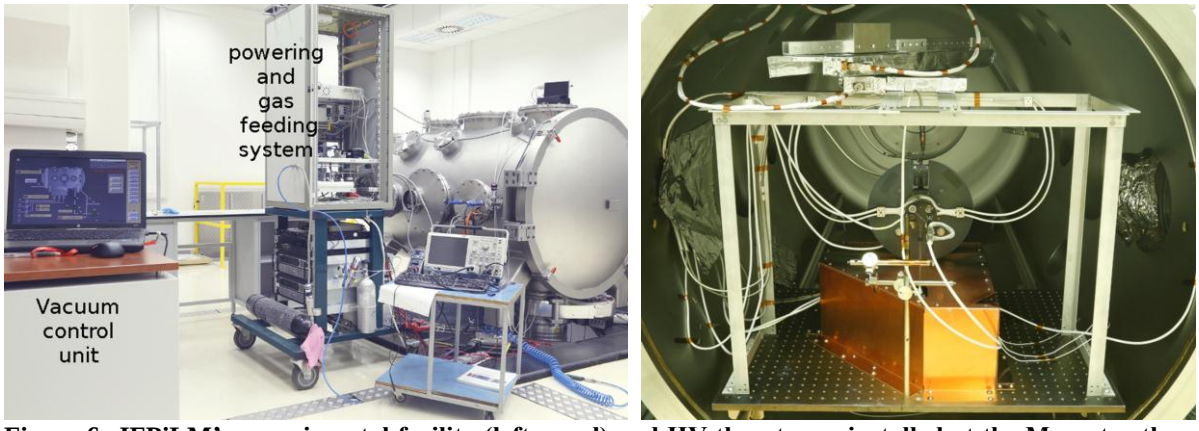

Figure 6. IFPiLM's experimental facility (left panel) and HV thruster as installed at the Mecartex thrust stand inside vacuum chamber (right panel). Above the thruster a system for angular and linear driving of diagnostics (e.g. electric probes) is mounted at a dedicated scaffolding.

[*] MECARTEX, https://www.mecartex.ch/news/

[†] Innovative Liquid Micro Pulsed Plasma Thruster system for Nanosatellites, EC FP7 project, GA No. 283279

It appeared however, that a built-in contactless (with respect to the pendulum) voice coil which was well suited for PPT, could not produce a reliable calibrating pulse for thrust measurement at the level of few millinewtons. As a remedy an external electro-mechanical calibrator was designed for parallel to the thrust vector force generation (with magnitude of 15.96(31) mN) by vertical displacement of a precisely weighted mass sample. The TB response (as recorded by the TB control software) to a sequence of 5 calibrating pulses produced with this electro-mechanical system is reproduced in Fig. 7. A slow inclination of the baseline illustrates the long term TB drift which in our measurement routine is taken into account by numerical procedure – see section Methodology.

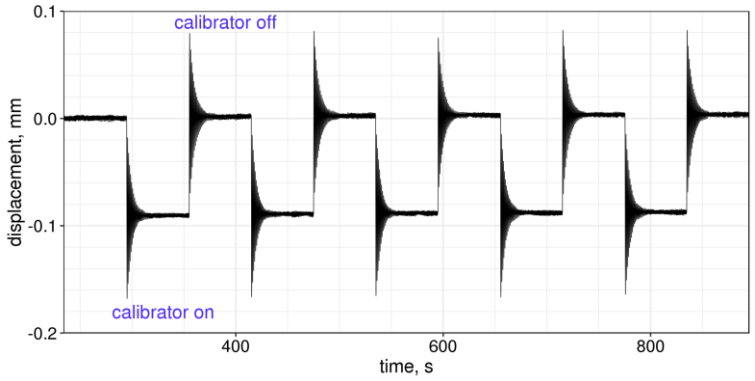

Figure 7. Sequence of thrust balance calibrating pulses indicating repeatability as well as signal to noise ratio.

D. Diagnostics

For thruster performance assessment standard measurements of the thruster current-voltage (*C-V*) characteristics were performed. The averaged in time signals and slowly variable parameters like coil currents and temperatures, keeper current and voltage etc. were recorded with data acquisition system consisted of two 8-channel DATAQ DI-730 units. Discharge current waveforms were measured with Tektronix TCP0030 current probe while thruster floating potential with Tektronix P5100A high voltage probe, both connected to DPO4104B 4 channel 8 bit Tektronix oscilloscope. The same oscilloscope was used for ion current recording as collected by a Faraday cup towards reconstruction of ion current density angular distributions (ICDAD) as well as for time-of-flight-analysis.

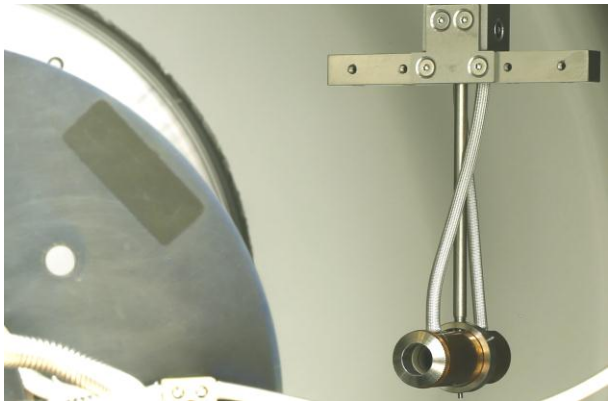

Figure 8. Collimated Faraday cup as install at the diagnostics driving system. The back of the thruster radiator is visible.

A collimated Faraday cup (FC) with diameter of the collimator equal to 10 mm and collecting diameter of the collector equal to 14 mm was designed and manufactured in IFPiLM. This type of ion probe was chosen as it enables to capture charged particles from the well-defined solid angle[18,19]. Moreover, the collimated FC, in comparison to planar Faraday probe, is less sensitive to low energy charge exchange (CEX) ions, the number of which depends heavily on the chamber background pressure. The FC collector was made of graphite which is known of reduced secondary electron emission yield with respect to typical metals and which machining is easy. The Faraday cup was installed at the arm of driving system allowing for its angular displacement in the range of ±90° with respect to the thruster axis – see Figs. 6 and 8. The center of rotation coincided with the thruster exit plane and the semicircle radius for FC displacement was set to 43.8 cm. The FC casing and collimator were left floating whereas the collector was polarized with voltage of -18 V. It was verified that variation of the collector voltage in the range of -5 to -45 V did not vary the magnitude of the average current collected by FC positioned at any angle in the whole range of thruster operating conditions.

III. Methodology

As it was mentioned in the Introduction one of the aims of the current study was revealing an operating envelope of the 0.5 kW class krypton HT when biased with high voltage for identification of the operating parameters at which high I_{sp} could be generated. To do this, discharge voltage was varied from 240 V up to 800 V and krypton mass flow rate from 0.6 mg/s up to 1.0 mg/s. For each set-point both coil current values and their ratio were adjusted in a wide range to maximize thruster efficiency which was usually equivalent to discharge power P_d minimization.

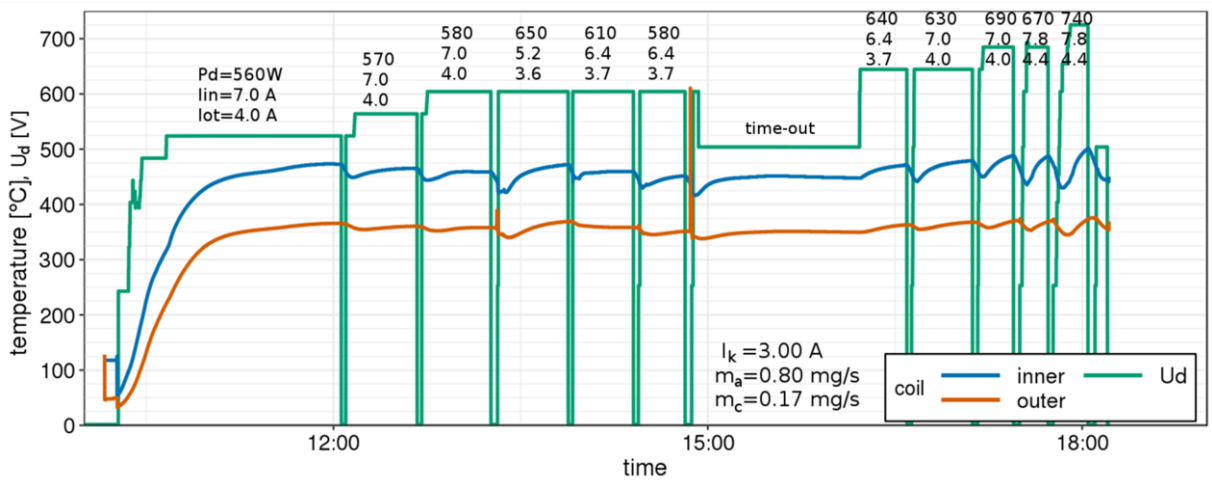

Figure 9. Thermal history of the kick-off HKHET version during one day of measurements. Inner (in blue) and outer (in orange) coil temperature variations are shown. Additionally discharge voltage is depicted (in green). Keeper current and mass flow rates were kept constant while coil currents were adjusted to minimize discharge power – each parameter variation is labeled with resulting discharge

It is obvious that discharge voltage U_d increase has to result in P_d growth (and thus power transferred to the thruster body) for constant mass flow rate, even assuming constant discharge current I_d. On the other hand, reduction of mass flow rate decreases I_d and consequently, discharge power. That is why, to avoid overpowering the thruster, usually only lower mass flow rates were examined at the highest U_d values.

All the measurements were performed only for the thruster thermally stable state which was identified by measurement of average temperatures of both coils. These temperatures were determined relying on coil resistivity variation during the thruster operation and assuming linear temperature relation for specific resistance of the winding wire. When the temperature of the windings approached too close to 500°C, the operating parameters were modified or even discharge switched off in order to cool down the thruster. A typical long term record of both coils temperature and discharge voltage is shown in Fig. 9. Zero voltage values correspond to intentional switching the thruster off for thrust value evaluation.

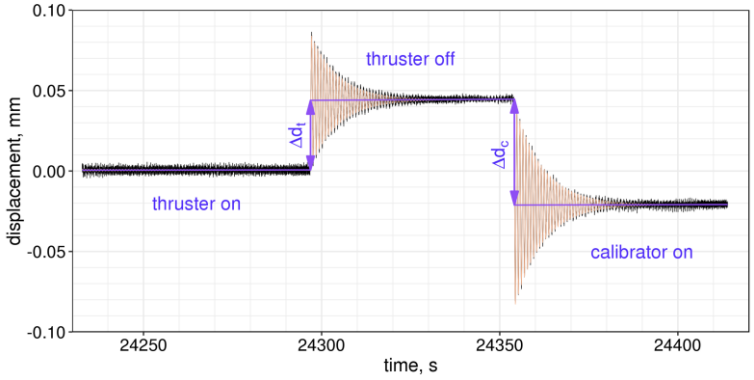

Figure 10. Displacement of thrust balance pendulum for thruster-on, thruster-off and calibrator-on cycle (black). A fitted damped oscillator with drift solution is shown in orange.

The measurement procedure consisted of a three-step sequence: 1 minute of thruster stable operation (when in thermally stable state), 1 minute of thruster switched off, and 1 minute of calibrating impulse switched on. To the signal from each step a damped harmonic oscillator function with drift $f(t) = A\cos(\omega t)\,\mathrm{e}^{-\gamma t} + at + b$ was fitted with least squares method (Levenberg-Marquardt).

The measurement routine is illustrated in Fig. 10 in which a sequence of thruster switch off and calibrator on events is reproduced together with the fitted analytical solution. Having the fit and the known calibrating force, the thrust was calculated from the ratio of the displacements $F_{\mathrm{thruster}} = F_{\mathrm{calibrator}} \frac{\Delta d_t}{\Delta d_c}$.

The standard uncertainty of the resulted thrust $u_{\mathrm{Fthruster}} = F_{\mathrm{thruster}} \sqrt{\left(\frac{u_{\mathrm{Fcalibrator}}}{F_{\mathrm{calibrator}}}\right)^2 + \left(\frac{u_{\Delta dt}}{\Delta d_t}\right)^2 + \left(\frac{u_{\Delta dc}}{\Delta d_c}\right)^2}$ consisted of three components: calibrating force uncertainty $u_{\mathrm{Fcalibrator}}$ of 0.31 mN and the uncertainties of the thruster

displacement $u_{\Delta dt}$ and calibrator displacement $u_{\Delta dc}$ (both of which depended on the fit quality that differed from case to case). Typically, the final TB uncertainty was of the order of 2%.

Faraday cup measurements were performed for ICDAD reconstruction, total ion current and its divergence assessment as well as for time-of-flight-analysis aimed at approximate mean ion velocity estimation towards voltage utilization rating. The waveform of the ion current at the axis of the thruster (at 0° angle) – if measured – was recorded simultaneously with discharge current waveform. Next, 100 seconds lasting forward and backward angular sweep (with speed of 4.5°/s) was activated for ICDAD reconstruction. In the latter case, the FC signal was recorded using additional analog filter for noise reduction to increase the oscilloscope gain for better ion current profile recovery. It is worth noting that for ICDAD reconstruction ion current profile was also corrected using geometrical scale factor adapted from Refs. 18 and 20.

Having ion signals recorded, the thruster was switched off for the thrust vector computation in accordance with the described above routine. Finally, the thruster was switched on again and a new set point was examined.

IV. Results and discussion

During the measurement campaign of the HIKHET first prototype the thruster's operating envelope was probed in a wide range of settings that included not only the typical operating parameters like mass flow rate, discharge voltage or magnetic field topography but also different hardware configurations like channel insulator shape, anode position or magnetic poles shape. Below presented are the major results obtained in this measurement campaign for two hardware settings that were described in section Thruster.

A. Performance

The discharge-voltage characteristics are presented in Fig. 11. Due to magnetic coil currents adjustments the data points appear quite scattered, that is why to each mass flow rate a smooth curve was fitted with loess method for easier viewing. Some of the points that went beyond the 700 W hyperbola were recorded when the thruster temperature was still increasing – however, by no more than 5°C/min – see Fig. 9. Significant difference between the two configurations can be seen: in the basic setting the mean discharge current lowered or stayed approximately the same as the voltage was increased (with the exception of 0.6 mg/s for which the curve exhibits a minimum) whereas in the final one the current grew. Little information on Hall Thrusters operated with krypton at high voltage can be found and compared with this result. In Ref. 8, where an SPT-100 fed with krypton was operated from 242 up to 574 V for several mass flow rates (from 3.27 to 5.72 mg/s), the anode current was rising very slowly – about 2.5% increase of discharge current over 332 V. However, in Ref. 5 an SPT-100 also operated with krypton (5 mg/s) up to 550 V showed current-voltage characteristic very similar to our thruster. In Ref. 10 krypton current-voltage curves are shown for an SPT-50 – device of similar channel geometry to HIKHET – but only up to 250 V. There, after a rapid increase of current starting from low voltage, the discharge current seemed to saturate which did not occur in our case. It should be noted, however, that the authors fed the SPT-50 with 1.12 to 1.77 mg/s of gas – significantly larger mass flow rate than in our experiment.

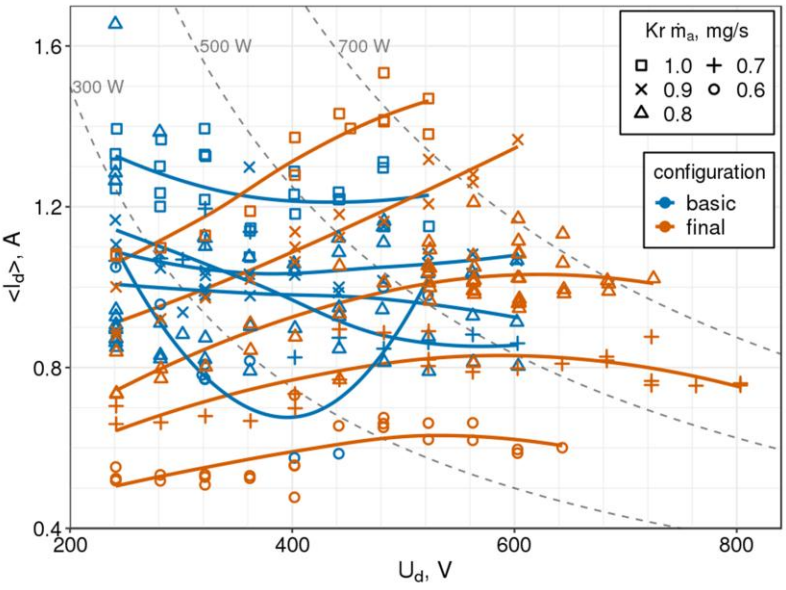

Figure 11. Mean discharge current as a function of discharge voltage. Curves were fitted with loess method. Several discharge power hyperbolas are also shown for reference.

It was noticed that at voltage of around 440 V and beyond the thruster could switch to a different operating mode that exhibited slightly larger discharge current and resulted in increased thrust production. This change in thrust is illustrated in Fig. 12.a. The theoretical relation $T \propto \sqrt{U_d}$ was well preserved and so it was possible to unambiguously fit square root-

type curve to each of the two performance regimes. The switch occurred for most tested mass flow rates but only for some magnetic coil currents settings – usually such that lowered the magnetic field magnitude. However, the cause of the presence of such two modes is unknown. The thrust measurements in the 'high' performance regime were positively verified using calibrating signals from 'low' performance, so this was proved to not be the effect of faulty measurements. It is interesting to notice that for the basic configuration in 'high' performance regime both intercept and slope became larger whereas for the final configuration the slope changed only little. Nevertheless, plotting the thrust versus a product of mass flow rate and square root of voltage (Fig. 12.b), it can be seen that the thrust production in the final hardware configuration of the thruster was more consistent.

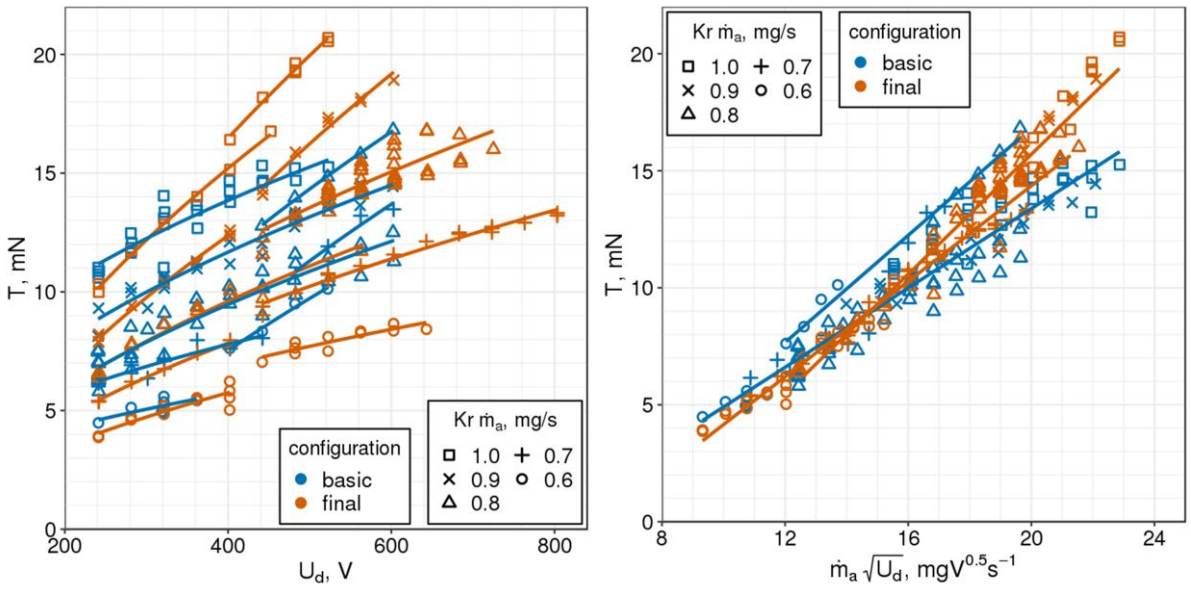

a) **b)**

Figure 12. Thrust as a function of a) discharge voltage, and b) product of mass flow rate and square root of discharge voltage. A square root (a) and linear (b) functions were fitted to each of the two performance regimes.

To obtain the full picture of the thruster performance it is important to relate the thrust production (and the resulting specific impulse) to the required discharge power. It is convenient to do this in a plot of thrust-to-power ratio as a function of specific impulse. There anode efficiency η_a hyperbolas ($\frac{T}{P_d} = \frac{2}{g_0}\frac{T^2}{2\dot{m}_a P_d}\frac{g_0\dot{m}_a}{T} = \frac{2}{g_0}\eta_a\frac{1}{I_{sp}}$) and specific input energy $\frac{P_d}{\dot{m}_a}$ lines ($\frac{T}{P_d} = g_0\frac{\dot{m}_a}{P_d}\frac{T}{g_0\dot{m}_a} = g_0\left(\frac{P_d}{\dot{m}_a}\right)^{-1} I_{sp}$) can be drawn for reference. The measured thruster performance envelope in two hardware settings is shown in such a graph in Fig. 13. First of all, it should be noted that in the optimized configuration we were able to consistently obtain specific impulse values of over 1800 s with maximum exceeding 2100 s. On the other hand, although in the final hardware setting the anode efficiency was improved compared to the basic one, the maximum efficiency was 30% at discharge power of 700 W. For comparison, the SPT-50M thruster operated with xenon propellant at similar power achieved anode efficiency of around 38% - Ref. 27. Figure 13 shows that in order to obtain even higher specific impulse at a reasonable power level (i.e. below 700 W) a significant improvement of thruster efficiency must be achieved.

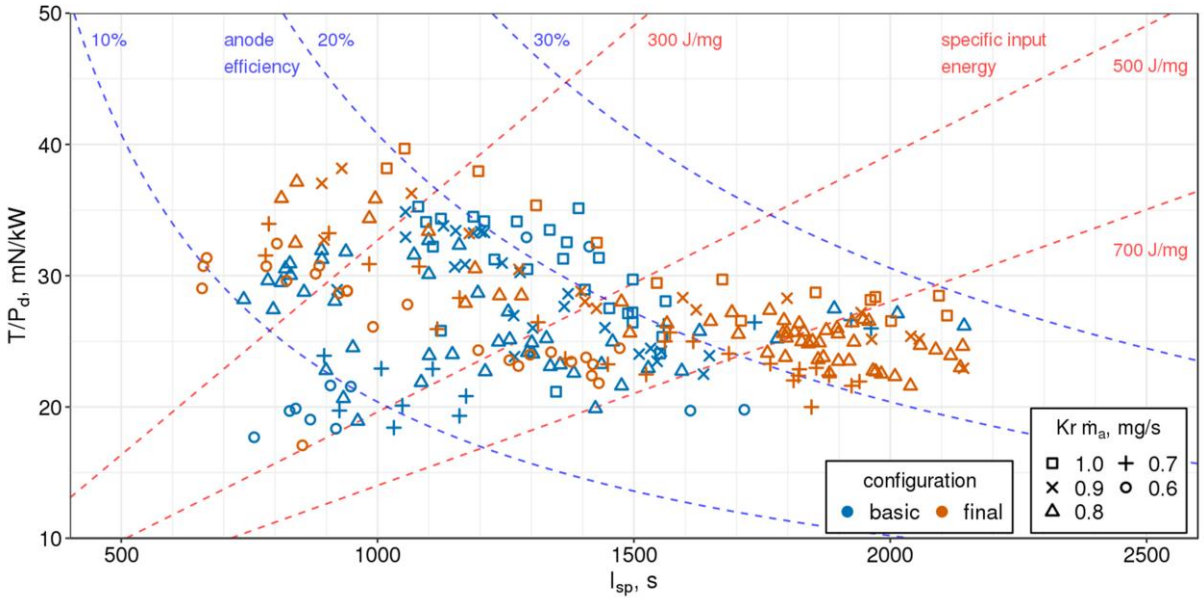

Figure 13. Thrust to discharge power ratio as a function of specific impulse. Several anode efficiency hyperbolas and specific input energy lines are also shown for reference.

B. Faraday Cup measurements

To better understand how the anode efficiency is reduced in our thruster, beam divergence and ion current were calculated basing on the ion current density angular distributions measured for the final configuration with Faraday Cup. Three such distributions measured at different discharge voltages are reproduced in Fig. 14 in linear and logarithmic scale. It can be noted that the ion current profiles exhibit small contribution of charge exchange ions perhaps thanks to relatively low pressure inside the vacuum chamber during thruster operation. The distributions were integrated to obtain the total ion current I_i and beam divergence efficiency η_div using the following formulas:

$$I_\mathrm{i} = \int_{-\pi/2}^{\pi/2} j_\mathrm{i} |\sin\theta| d\theta \tag{1}$$

$$\eta_{div} = \langle \cos\theta \rangle^2 = \left(\frac{\int_{-\pi/2}^{\pi/2} \cos\theta \, j_\mathrm{i} |\sin\theta| d\theta}{\int_{-\pi/2}^{\pi/2} j_\mathrm{i} |\sin\theta| d\theta} \right)^2 \tag{2}$$

where j_i is the ion current density in mA/sr and θ is the angle between the thruster and FC axes. Both are shown in Fig. 15. Relatively wide spread of obtained values is the outcome from the assumed methodology according to which magnetic coil currents were varied searching for maximum thruster performance. Nevertheless, it is clear that beam divergence decreases (i.e. beam divergence efficiency increases) with the growth of discharge voltage.

Having the total ion current, the current utilization (i.e. ion current to discharge current ratio $I_\mathrm{i}/I_\mathrm{d}$) was determined and is shown in Fig. 16.a. In the whole range of tested voltages this ratio was mostly between 0.50 and 0.65 with no clear trend visible. These values are significantly lower than 0.8 that is reported for SPT-100 operated with xenon[10] or 0.9 for NASA-173Mv1 operated with krypton[7] (although these are significantly bigger thrusters) which hints at the possibility of poor electron confinement that leads to increased contribution of electron current.

To assess how well the gas supplied to the thruster is utilized the measured ion current can be also compared with the maximum current I_m of singly-charged ions for the given mass flow rate, i.e. $I_\mathrm{m} = e\dot{m}_\mathrm{a}/M$, where M is the ion mass. However, the ratio of $I_\mathrm{i}/I_\mathrm{m}$ can serve only as an estimate of the mass utilization efficiency because of the presence of multiply-charged ions (which increase in number at higher voltages). As shown in Fig. 16.b, this ratio was in the range from 0.4 to 0.5 at 240 V (comparable with the $I_\mathrm{i}/I_\mathrm{m}$ ratio of about 0.5 reported for SPT-50 operated with krypton at 250 V – Ref. 10) and increased to above 0.6, but it is unknown how much this rise was influenced by multiply-charged ions. It means, however, that the mass utilization must be lower than 0.6. For comparison, the mass utilization efficiency in large Hall Thrusters operated with krypton is reported to be as high as 0.85 – Ref. 7.

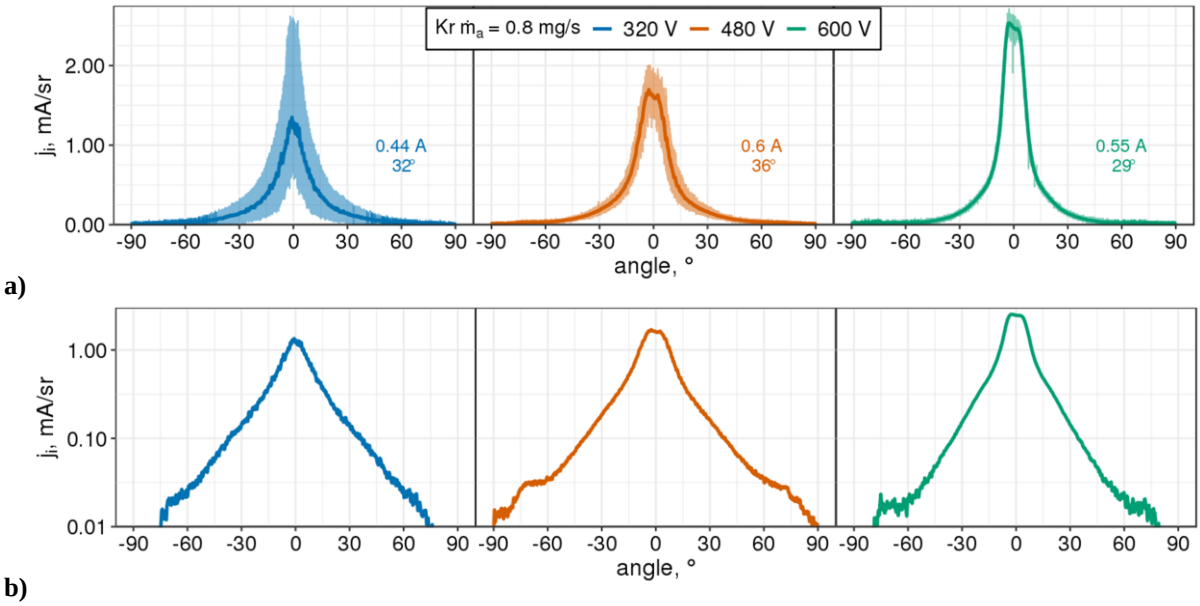

Figure 14. Ion current density angular distributions of the final configuration in a) linear, and b) logarithmic scale. Shaded lines represent raw Faraday Cup signal and solid lines show signal filtered using Savitzky-Golay method with 1.8° filter length. To the right of the profile are shown the integrated values: total ion current and beam divergence.

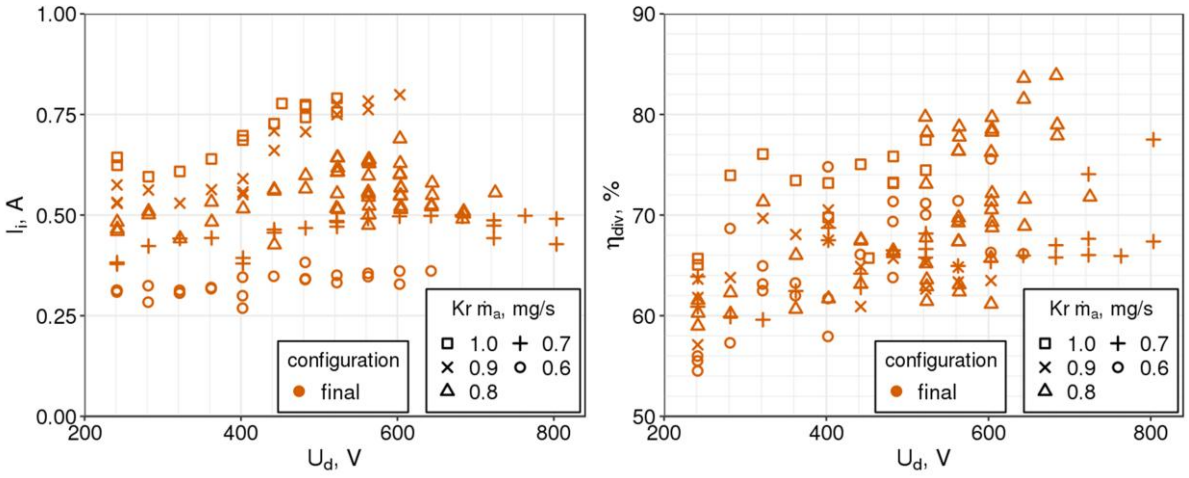

Figure 15. a) Ion current, and b) beam divergence efficiency as functions of discharge voltage.

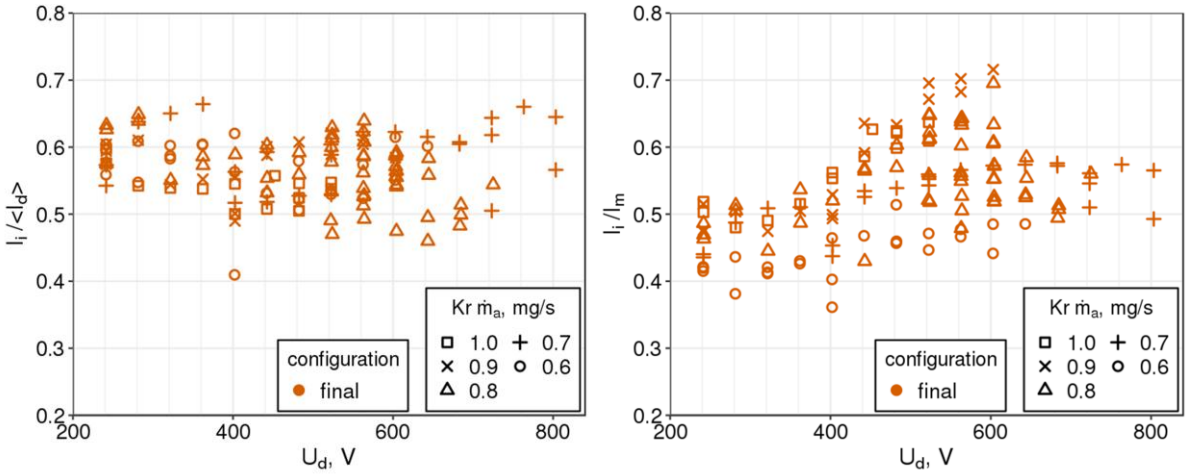

a) **b)**

Figure 16. a) Ion current to mean discharge current ratio, and b) ion current to maximum singly-charged ion current ratio as functions of discharge voltage.

The same Faraday Cup diagnostics was utilized to estimate the ion velocity using time-of-flight approach. The signals of discharge current and FC collector ion current were normalized to zero mean and unit variance, and then correlated with different time lags (cross-correlated) to yield the time needed for the ions to travel the known distance of 43.8 cm from the thruster to the FC. The distance divided by this time was used as an estimate of the mean ion velocity at the thruster axis. The procedure is illustrated in Fig. 17. This type of measurements was performed only for the final hardware configuration and three mass flow rates.

The estimated in this way ion velocities are shown in Fig. 18.a. These velocities are significantly greater than those which can be derived from specific impulse (e.g. 33 km/s from time-of-flight approach versus 19 km/s from specific impulse for 0.8 mg/s at 800 V) because the latter averages this velocity over the whole mass supplied to the thruster. Nevertheless, calculation of the effective accelerating voltage necessary to speed up ions to such velocities (assuming singly-charged ions) reveals that voltage utilization in most cases was below 0.6, as shown in Fig. 18.b. For comparison, for NASA-173Mv1 with krypton voltage utilization can be as high as 0.8 – Ref. 7.

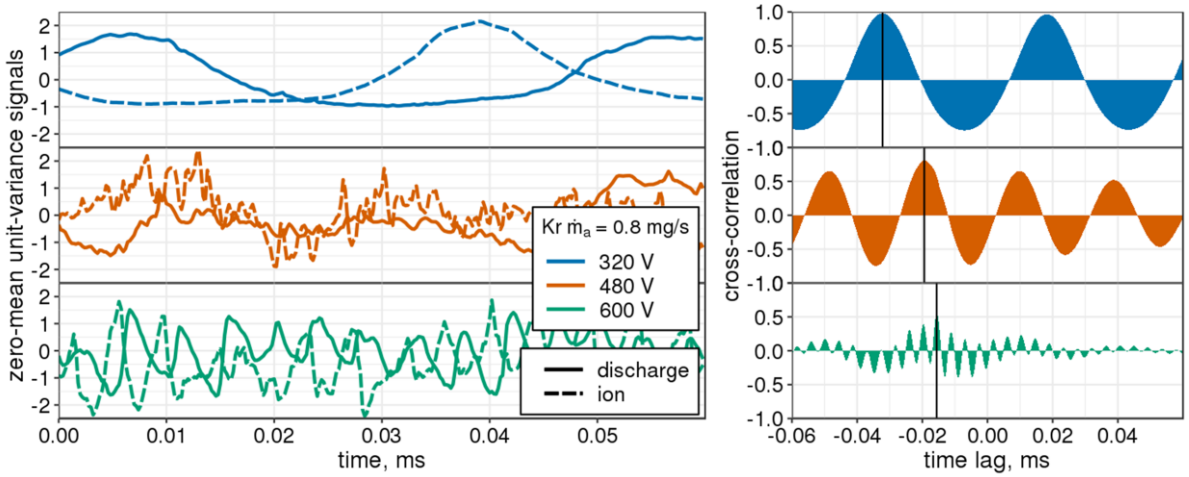

a) **b)**

Figure 17. a) Discharge and ion current waveforms, and b) cross-correlation of these signals. The vertical lines in the right sub-figure correspond to maximum correlation and thus estimated time-of-flight.

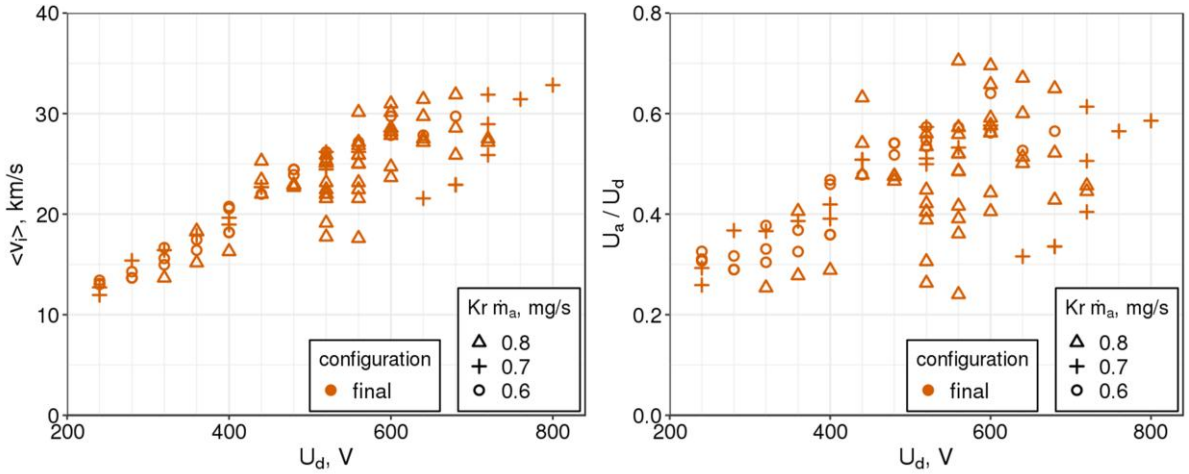

a) **b)**

Figure 18. a) Estimated mean ion velocity, and b) resulting accelerating-to-discharge voltages ratio as functions of discharge voltage.

C. Ion current oscillations

It is well known that even subtle distortion of relations between mass flow rate, discharge voltage and magnetic field magnitude may result in significant change of discharge current oscillations character which is interpreted as transition between global (including breathing-type) and local modes[21,22]. Such transitions were also observed to appear as catastrophe[23] causing increase of discharge current mean value and/or amplitude of I_d oscillations what results in thruster performance degradation. In our thruster such transitions were observed to happen without noticeable reason when thruster was approaching thermal steady state. It is supposed that slow modification of magnetization curve due to growth of temperature, and thus B-field topography, could be responsible for evident switch in observed discharge current oscillations character.

In this study also Faraday Cup was used to provide insight into stability and characteristic frequencies of discharge fluctuations when thruster is operated at different voltages and coil currents. Despite that spectral content of non-stationary and non-linear signals should be determined with dedicated methods like wavelet transform and/or empirical mode decomposition (EMD) accompanied by Hilbert-Huang transform for marginal spectra calculations[24,25], the traditional Fourier techniques, when applied with caution, are also able to provide valuable information. For simplified spectral analysis the same ion current and discharge current signals as for correlation analysis were used. They were recorded during 20 ms with 5 MHz sampling rate (Nyquist frequency 2.5 MHz). Calculated power spectral densities (PSD) represent three characteristic types of signals: a) semi-periodic signals with leading frequency from the range of 20-30 kHz and quickly decreasing share of harmonics, b) broadband signals fluctuating around frequency from the range of 30-40 kHz and c) signals in which significant peak of frequency about 5 to 10 times higher than in case a) and b) appears. The corresponding PSDs are reproduced in Fig. 19. It is interesting that when thruster was operated at high U_d the share of low frequency oscillations in PSD of ion current density was significantly reduced in comparison with PSD calculated for I_d. The well pronounced peak with maximum ~250 kHz that is visible in both PSDs for U_d=600 V is likely to represent ion transit time oscillations, i.e. the oscillations with the characteristic frequency corresponding to time-of-flight of ions through the acceleration zone. Oscillations of this type were unambiguously identified applying EMD method for marginal spectra calculation[26]. In our case the relative power of this oscillation identified in discharge current and Faraday Cup signals is comparable (both signals were normalized to zero mean value and unit variance) – moreover, in both signals this oscillation faded if discharge voltage decreased.

To illustrate temporal evolution of power spectral density and stability of the leading frequency a simple method of STFT (Short-Time Fourier Transform) was applied for both signals. The resulting spectrograms for mass flow rate of 0.8 mg/s are depicted in Fig. 20. The width of each spectrogram calculated for different discharge voltage and coil currents (a stripe in this figure) corresponds to time interval of 20 ms. The whole signals composed of 10^5 data points were binned using Blackman window with the length of 5000 elements. With sampling frequency of 5e3 kHz the frequency resolution Δf=1 kHz and time resolution Δt=1 ms was provided. In Fig. 20 it can be seen that the leading frequencies fluctuate in time in both discharge and ion current signals. The range of these fluctuations

increased with voltage – however, could be partially stabilized due to adjustment of coil currents. For higher discharge voltage values low frequency components (below 10 kHz) seemed to appear in ion current signal at random. The corresponding frequency bands were only poorly identified in the discharge current signal.

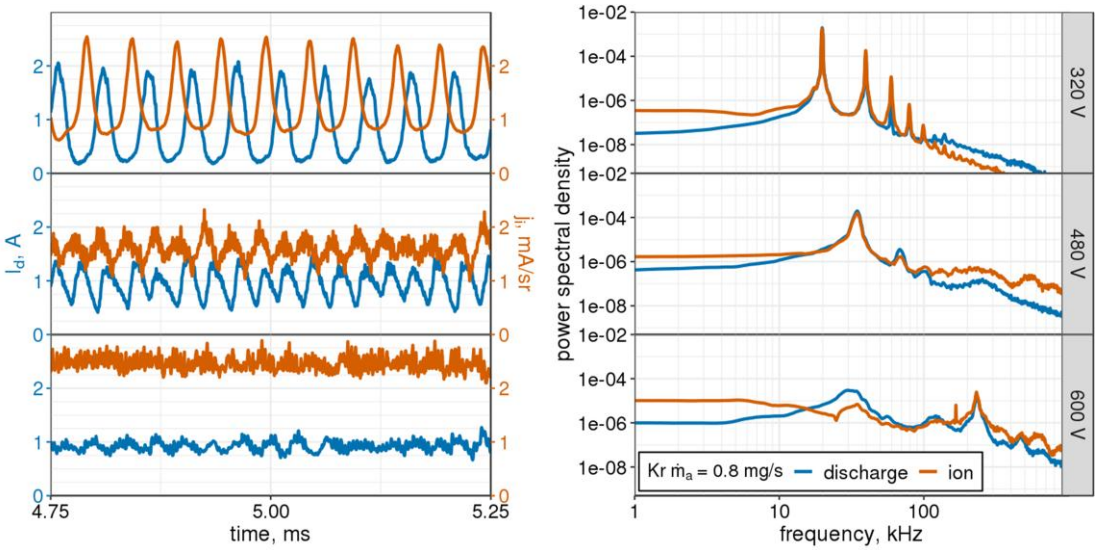

Figure 19. Discharge and ion signals in time and frequency domains for three discharge voltages. PSDs were calculated from 20 ms-long signals using adaptive sine multitaper method.

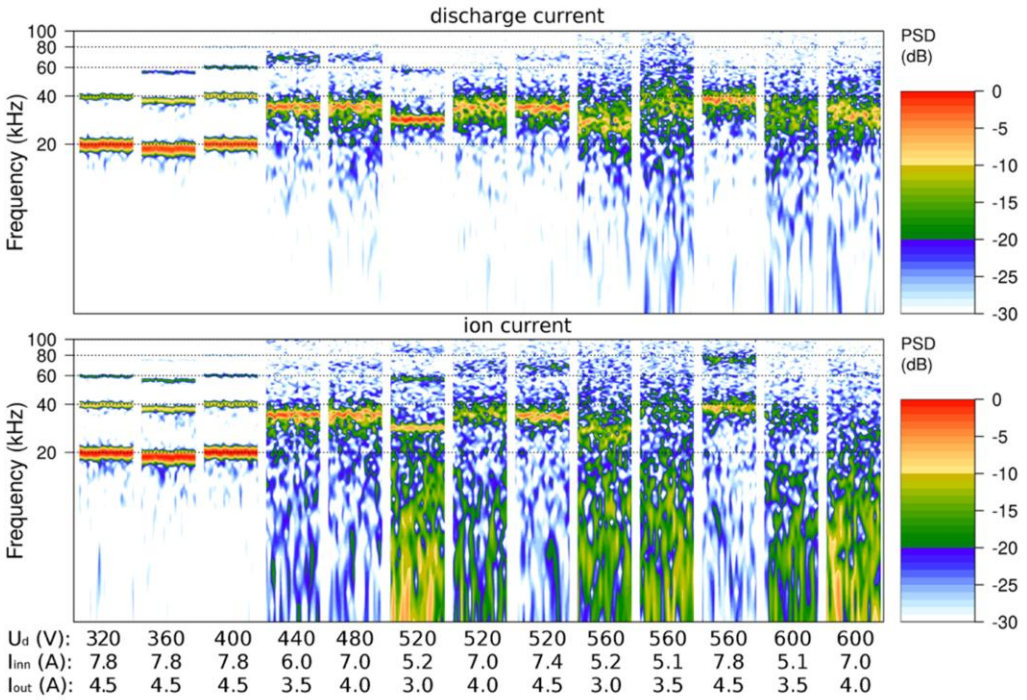

Figure 20. Spectrographic representation of discharge current and ion current signals for different operation parameters at 0.8 mg/s mass flow rate. The width of each spectrogram is 20 ms.

D. Channel erosion

During the experimental campaign it was noticed that the thruster exhibits fast erosion of the channel insulator. The 3 mm-thick inner wall became almost completely eroded after 214 hours of operation, as shown in Fig. 21. Such erosion rate is not unusual however, because in an SPT-40 operating with krypton at mass flow rates from 0.86 to 1.05 mg/s and voltage of up to 310 V a 2 mm-thick inner wall eroded away after less than 150 hours[11].

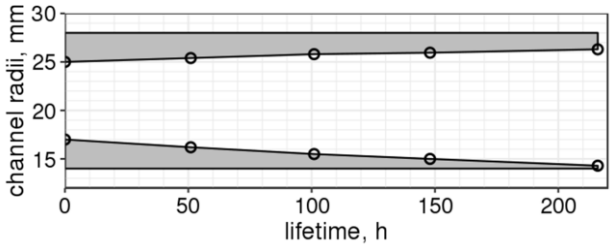

a)

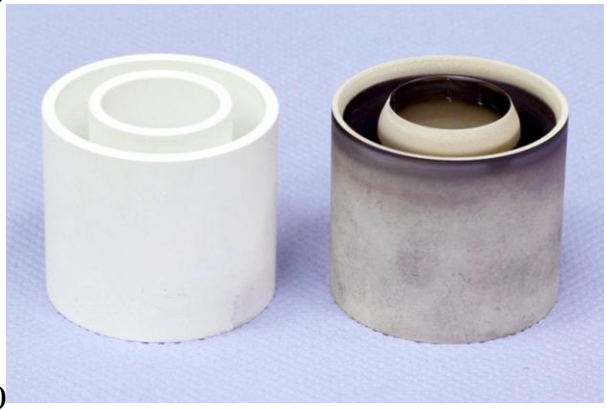

b)

Figure 21. Erosion of the plain channel insulator. a) History of erosion at the channel exit. b) Comparison of new and eroded insulators.

In our case the increased erosion rate probably stemmed from the fact that the thruster was operating in a highly varied magnetic field settings and at high voltages. As a consequence, non-optimal magnetic field topographies and large ion energies could have led to intense wall bombardment. However, low mass and voltage utilization that was obtained from Faraday Cup measurements in the whole range of tested operating conditions suggest another scenario as the main factor of fast erosion. As was shown in Fig. 5, the ionization-acceleration zone in our thruster reaches quite deep inside the channel. This is confirmed by the depth of the erosion which coincides with the upstream boundary of this zone. Consequently, the ions that are produced first are formed deep inside the channel from where they have high probability of hitting the channel walls as they are accelerated downstream. By hitting the wall they are neutralized and may be ionized again or may leave the thruster as neutrals leading to decreased mass utilization. Moreover, a large portion of accelerating voltage (and energy) in this process is lost from the point of view of thrust generation and instead used for wall bombardment, resulting in observed low voltage utilization. To reduce the channel erosion and improve mass and voltage utilization a new magnetic field topography should be introduced, such that will move the ionization-acceleration zone further downstream.

V. Conclusion

The first prototype of HIKHET – a high-impulse 500 W-class small Hall Thruster fuelled with krypton – was successfully operated up to 800 V. Specific impulse of over 2000 s was demonstrated, but the anode efficiency did not exceed 30%. This may be related with observed high erosion rate as well as unsatisfactory current and voltage utilization efficiencies. As a next step, a second prototype of HIKHET will be designed with improved magnetic field topography to limit the ion losses at the channel walls and to allow further increase of obtainable specific impulse.

Acknowledgments

Project HIKHET is carried out under a programme of, and funded by, the European Space Agency since January 2018, Contract No. 4000122415/17/NL/GE. Project KLIMT was supported by ESA in the frame of the second PECS call (Contract No. 4000107746/13/NL/KLM) in years 2013-2016. The view expressed in this publication can in no way be taken to reflect the official opinion of the European Space Agency. The project LμPPT was funded by the European Comission (FP7 project, No. 283279) and received support from the Foundation for Polish Science in years 2012-2014.

References

[1]Leporini, A., Giannetti, V., Andreussi, T., Pedrini, D., Rossodivita, A., Piragino, A., Andrenucci, M., and Estublier, D. "Development of a 20 kW-class Hall effect thruster," *Space Propulsion 2016*, CP-3125196, 2016.

[2]Lee, E., Kim, Y., Lee, H., Kim, H., Doh, G., Lee D., and Choe W., "Scaling approach for sub-kilowatt Hall-effect thrusters," *Journal of Propulsion and Power*, 2019. doi:10.2514/1.B37424

[3]Loyan, A. V., and Maksymenko, T. A., "Performance investigation of SPT-20M low power Hall effect thruster," *Journal of Technical Physics*, Vol. 49, No. 3-4, 2008, pp. 283-302.

[4]Ahedo, E., and Gallardo, J. M., "Scaling down Hall thrusters," *28th International Electric Propulsion Conference*, IEPC-2003-104, 2003.

[5]Kim, V., Popov, G., Kozlov, V., Skrylnikov, A., and Grdlichko, D., "Investigation of SPT Performance and Particularities of it's Operation with Kr and Kr/Xe Mixtures," *27th International Electric Propulsion Conference*, IEPC-01-065, 2001.

[6]Kieckhafer, A., and King, L. B., "Energetics of Propellant Options for High-Power Hall Thrusters," *Journal of Propulsion and Power*, Vol. 23, No. 1, 2007, pp. 21-26. doi: 10.2514/1.16376

[7]Linnell, J. A., and Gallimore, A. D., "Efficiency Analysis of a Hall Thruster Operating with Krypton and Xenon," *Journal of Propulsion and Power*, Vol. 22, No. 6, 2006, pp. 1402-1412. doi: 10.2514/1.19613

[8]Nakles, M. R., Hargus Jr., W. A., Delgado, J. J., and Corey, R. L., "A Performance Comparison of Xenon and Krypton Propellant on an SPT-100 Hall Thruster," *32nd International Electric Propulsion Conference*, IEPC-2011-003, 2011.

[9]Bugrova, A. I., Bishaev, A. M., Desyatskov, A. V., Kozintseva, M. V., Lipatov, A. S., and Dudeck, M., "Experimental Investigations of a Krypton Stationary Plasma Thruster," *International Journal of Aerospace Engineering* ,Vol. 2013, 686132, 2013. doi: 10.1155/2013/686132

[10]Kim, V. P., Zakharchenko, V. S., Merkur'ev, D. V., Smirnov, P. G., and Shilov, E. A., "Influence of Xenon and Krypton Flow Rates through the Acceleration Channel of Morozov's Stationary Plasma Thruster on the Thruster Efficiency," *Plasma Physics Reports*, Vol. 45, No. 1, 2019, pp. 11-20. doi: 10.1134/S1063780X19010082

[11]Saevets, P. A., Kim., V. P., Grdlichko, D. P., and Smirnov, P. G., "Investigation of a Low-power Thruster on Krypton Propellant," *Procedia Engineering*, Vol. 185, 2017, pp. 85-90. doi: 10.1016/j.proeng.2017.03.296

[12]Kurzyna, J., Szelecka, A., Daniłko, D., Barral, S., Dannenmayer, K., Bosch Borras, E., and Schönherr, T., "Testing KLIMT prototypes at IPPLM and ESA Propulsion Laboratories," *Space Propulsion 2016*, CP-3125256, 2016.

[13]Kurzyna, J., Jakubczak, M., Szelecka, A., and Dannenmayer, K., "Performance tests of IPPLM's krypton Hall thruster," *Laser and Particle Beams*, Vol. 36, No. 1, 2018, pp. 105-114. doi:10.1017/S0263034618000046

[14]Zhurin, V. V., Kaufman, H. R., and Robinson, R. S., "Physics of closed drift thrusters," *Plasma Sources Science and Technology*, Vol. 8, No. 1, 1999, pp. R1-R20. doi: 10.1088/0963-0252/8/1/021

[15]Mitrofanova, O. A., and Gnizdor, R. Y., "Influence of SPT magnetic field on life time characteristics of the thruster," *33rd International Electric Propulsion Conference*, IEPC-2013-51, 2013.

[16]Kim, V. P., Gnizdor, R. Y., Grdlichko, D. P., Merkuriev, D. V., Mitrofanova, O. A., Smirnov, P. G., Shilov, E. A., and Zakharchenko, V. S., "Fundamental Principles Employed for Ionization and Acceleration Layer Control in the Discharge of a Stationary Plasma Thruster," *Journal of Surface Investigation: X-ray, Synchrotron and Neutron Techniques*, Vol. 12, No. 6, 2018, pp. 1237-1247. doi: 10.1134/S1027451018050610

[17]Barral, S., Kurzyna, J., Szelecka, A., Rachubiński, H., Remírez, E., Martín, R., Ortiz, P., Alonso, J., Bottinelli, S., Mabillard, Y., Zaldívar, A., Rangsten, P., and Koppel, C., "First experimental characterization of a pulsed plasma thruster with non-volatile liquid propellant," *Space Propulsion 2014*, CP-2980924, 2014.

[18]Hofer, R. R., Walker, M. L. R., Gallimore, A. D., "A Comparison of Nude and Collimated Faraday Probes for Use with Hall thrusters", *27th International Electric Propulsion Conference*, IEPC-01-020, 2001.

[19]Mazouffre, S., Largeau, G., Garrigues, L., Boniface, C., and Dannenmayer K., "Evaluation of various probe designs for measuring the ion current density in a Hall thruster plume", *35th International Electric Propulsion Conference*, IEPC-2017-336, 2017.

[20]de Grys, K. H., Tilley, D. L., and Aadland, R. S., "BPT Hall Thruster Plume Characteristics," *35th AIAA/ASME/SAE/ASEE Joint Propulsion Conference and Exhibit*, AIAA 99-2283, 1999.

[21]Hara, K., Boyd, I. D., Sekerak, M. J., and Gallimore, A. D., "Breathing mode in Hall effect thrusters," *34th International Electric Propulsion Conference*, IEPC-2015-283, 2015.

[22]Sekerak, M. J., "Plasma Oscillations and Operational Modes in Hall Effect Thrusters," Ph.D. Dissertation, Univ. of Michigan, 2014.

[23]Ding, Y., Su, H., Li, P., Wei, L., Li, H., Peng, W., Xu, Y., Sun, H., and Yu, D., "Study of the catastrophic discharge phenomenon in a Hall thruster," *Physics Letters A*, Vol. 381, No. 40, 2017, pp. 3482-3486. doi: 10.1016/j.physleta.2017.09.002

[24]Huang, N. E., and Wu, Z., "A review on Hilbert-Huang transform: Method and its applications to geophysical studies," *Reviews of Geophysics*, Vol. 46, No. 2, 2008. doi: 10.1029/2007RG000228

[25]Kurzyna, J., Mazouffre, S., Lazurenko, A., Albarede, L., Bonhomme, G., Makowski, K., Dudeck, M., and Peradzyński, Z., „Spectral analysis of Hall-effect thruster plasma oscillations based on the empirical mode decomposition," *Physics of Plasmas*, Vol. 12, No. 123506, 2005. doi: 10.1063/1.2145020

[26]Vaudolon, J., and Mazouffre, S., "Investigation of the ion transit time instability in a Hall thruster combining time-resolved LIF spectroscopy and analytical calculations," *34th International Electric Propulsion Conference*, IEPC-2015-400, 2015.

[27]Saevets, P., Semenenko, D., Albertoni, R., and Scremin, G., "Development of a Long-Life Low-Power Hall Thruster", *35th International Electric Propulsion Conference*, IEPC-2017-38, 2017.